Applications of $LiNbO_3$ Nested Waveguide and Design of AlGaAs Nested Waveguide for Terahertz Difference Frequency Generation

by

Chris Zenner

A project paper submitted in partial fulfillment of

the requirements for the degree of

Master of Science

(Electrical Engineering)

at the

UNIVERSITY OF WISCONSIN-MADISON

2011

Abstract

Nonlinear optics is the consequence of the nonlinear dependence of the polarization of a material on the incident electric field. Typically, to detect the nonlinear optical process the incident light must be relatively intense (~10^8 V/m) compared to the atomic fields. Because of this process, it is possible to develop light sources in frequency regimes where conventional methods no longer apply. In this project, the frequency of interest is ~1 - 3 THz.

There is a high amount of research in the terahertz regime (0.3 - 3 THz) because of the possible applications in military and national security. As a result, there is a high demand for room-temperature, compact, high power conversion efficiency, narrow-linewidth, continuous wave (CW) sources. One possible solution is multilayer nested waveguides. It has been shown that intense light sources can cause nonlinear effects in bulk material, but to significantly improve the optical power of the THz source, multilayer waveguide structures offer much higher optical confinement, single mode operation, improved overlap of pumps and THz, and tuning ability.

To model the IR and THz mode propagation in the multilayer, single mode waveguide, a beam propagation method (RSoft's BeamPROP) was used to calculate the effective index. The phase matching criteria discussed later in the paper was used to determine the frequency of the THz. The peak THz power was calculated by taking the overlap integral of the IR pump mode and THz mode. Because the model simulation worked accurately for the $LiNbO_3$ nested waveguide, a modified version was used for the AlGaAs nested waveguide.

Unfortunately, the current AlGaAs nested waveguide model did not produce the THz in the frequency range we calculated, and device limitations prevent the possibility of exploring higher frequency. The reason for the miscalculation could be from inaccurate index of refraction data for $Al_xGa_{1-x}As$, high absorption peaks at the THz frequency, and/or an incorrect nonlinear polarization coefficient.

Although the THz source did not produce measurable power at the scanned frequency range, it is still possible the device will produce THz at a higher frequency than current devices will allow. Therefore, in future research, it should be desirable to scan the upper frequency region above 4 THz.

Acknowledgements

During my years as an undergraduate and a graduate, I have had the unwavering support of several individuals that helped me along the way, both academically and caringly.

I would first like to thank my academic and research advisor, Professor Leon McCaughan. As an undergraduate, he gave me the opportunity to begin working in research in the field of optics and photonics that was relevant to current real-world applications. It was his motivation and advice that helped me to purse an advanced degree in Electrical Engineering. I will continue to appreciate the many discussions we had over the years, related to both current research projects and general life lessons.

I would like to thank my other research advisor, Professor Kuech, because it would not have been possible to perform the research without the hard work and dedication of him and his research students, most notably Steven Ruder. It was with their help and tolerating the many alterations we made to the AlGaAs waveguide system that made the research possible.

Without the help of undergraduate student and office mate Cedric Meyers, I would have been buried under an insurmountable quantity of research, papers, and presentations.

Of course it wouldn't have all been possible without the loving care and continued support from my parents Mary and Jim Zenner, who were always proud of my accomplishments.

And to my wife, Brittany, who came with me to Madison to encourage and support me through my schooling, during the most frustrating and the most joyous of occasions. It is with her unconditional love that will continue to give me the strength to push myself to my full potential.

Contents

Chapter 1

Introduction to Nonlinear Optics and SM waveguides

The frequency range greater than 1 THz has been of very intense research for years because of the strong rotational and vibrational properties of molecules, giving rise for the need of highly coherent, narrow linewidth, and stable sources. These strong and unique absorption lines have been under much research because of the potential application for explosives and drugs detection [1], plasma fusion diagnostics [2], and secure communications [3]. Currently, there are no compact, highly efficient, room temperature sources and detectors available for practical use. Also, there is a lack of devices to produce over 1 mW of narrow band light at 1 THz [4]. Recently, it has been demonstrated that a nested waveguide in a titanium diffused $LiNbO_3$ nested waveguide structure was able to produce highly coherent, continuous-wave (CW), and record power conversion efficiency than previous reported bulk nonlinear material [5]. Using a similar approach for the Ti:$LiNbO_3$ THz source, it is possible to achieve a higher conversion efficiency at ~ 3 THz by using the nonlinear semiconductor material GaAs by designing a multilayer nested waveguide structure in AlGaAs. The following sections will discuss the physics properties and necessary conditions to be met for difference frequency generated (DFG) THz radiation to be produced.

2nd Order Nonlinear Susceptibility

Nonlinear optical phenomenon that arise from light interaction with nonlinear materials is a product of the higher order susceptibilities, $\chi^{(2)}$, $\chi^{(3)}$... $\chi^{(N)}$ [6]. Linear materials only have a 1st order susceptibility, $\chi^{(1)}$, which is related to the index of refraction of a material by $n^2 = \chi^{(1)} + 1$, or if the incident E-field has a low intensity (< 10^8 V/m). The susceptibility of a material relates the polarization of the molecules ($\vec{P}$) and the applied electrical field ($\vec{E}$) by the relation

$$\vec{P}(t) = \varepsilon_o \chi^{(1)} \vec{E}(t) + \varepsilon_o \chi^{(2)} \vec{E}(t)^2 + \varepsilon_o \chi^{(3)} \vec{E}(t)^3 + ... \varepsilon_o \chi^{(N)} \vec{E}(t)^N \qquad (1.1)$$

where ε_o is the permittivity of free space. Since we are considering the nonlinear properties of materials, we will only be concerned with the second term. If we assume the electrical field is propagating as a plane wave (which for lasers it is typically not, but it will make the analysis simpler), it can be expressed as

$$\vec{E}(t) = Ee^{j(\omega t - kz)} + c.c. \qquad (1.2)$$

If we consider a single frequency laser source, we can see that polarization can be expressed as

$$\vec{P}(t)^{(2)} = \varepsilon_o \chi^{(2)} E^2 e^{j(2\omega t - 2kz)} + c.c. + 2\varepsilon_o \chi^{(2)} EE^* \qquad (1.3)$$

where the first and second term result in a new EM field at frequency 2ω, a nonlinear process know as second-harmonic generation. The third term is a static DC electric field in the material, a process known as optical rectification.

A more interesting case is the presence of two sources at different frequencies, ω_1 and ω_2. The resulting electric field has the same form as Eq. (1.2). Inserting the equations for the two

plane wave electric fields into the second term of Eq. (1.1) results in a polarization that consists of ten terms instead of three (Eq. 1.4).

$$P(t)^{(2)} = \varepsilon_o \chi^{(2)} \begin{pmatrix} 2E_1E_1^* + 2E_2E_2^* + \\ E_1^2 e^{j(2\omega_1 - 2k_1 z)} + c.c. + E_2^2 e^{j(2\omega_2 - 2k_2 z)} + c.c. + \\ 2E_1E_2 e^{j((\omega_1+\omega_2)t-(k_1+k_2)z)} + c.c. + \\ 2E_1E_2^* e^{j((\omega_1-\omega_2)t-(k_1-k_2)z)} + c.c. \end{pmatrix} \quad (1.4a\text{-}d)$$

where the first two terms in the first row are optical rectification (OR), the second row is second-harmonic generation (SHG), the third row is sum-frequency generation (SFG), and the fourth row is difference-frequency generation (DFG). The terms we will be concerned with are the DFG terms.

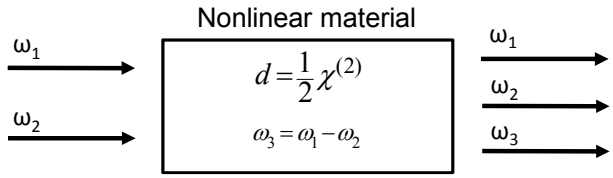

Figure 1.1. Schematic representation of DFG process

In the next section, we will discuss the conditions that must be satisfied to produce a DFG signal.

Phase Matching Condition for DFG

To generate a third signal, ω_3, there are two conditions that need to be met according to Eq. 1.4d. According to the conservation of energy, the total sum of the energy in a closed system has to equal zero. If we consider the two pump signals, ω_1 and ω_2, this means

$$\omega_3 = \omega_1 - \omega_2 \tag{1.5}$$

where if we replace each ω term with its corresponding energy, $E = hc/\lambda = h\omega/2\pi$, then we indeed get $E_3 = E_1 - E_2$. The second condition to be met is the phase between the pump signals and the DFG signal must be in phase, i.e. traveling through the material at the same speed so the generated signal at one point in the material adds in phase with the signal generated at a previous point in the material. For this to be true, the difference in the wavenumbers for the pumps (k_1-k_2) must be the same as the wavenumber for the generated signal (k_3), therefore

$$k_3 = k_1 - k_2 \tag{1.6}$$

or

$$n_1\omega_1 - n_2\omega_2 = n_{THz}\omega_{THz} \tag{1.7}$$

where $k = n\omega/c$. Since phase matching is difficult to achieve, especially over a long length of material, there is inherent phase mismatch and is given by

$$\Delta k = k_1 - k_2 - k_3 \tag{1.8}$$

where the ideal case is $\Delta k = 0$. Intuitively, we can see the degree of error involved in the DFG process is governed by the phase mismatch (which is determined by the refractive index of the signals in the material and the frequency of the signals) and the length of the material. Longer waveguides will require the phase fronts of the three signals to be at more similar velocities than shorter waveguides. The derivation of the phase mismatch factor can be derived by using the result of the polarization equations above and substituting them into Maxwell's wave equation and solving for the field intensity [7]. We will only report the result, which has the form $\mathrm{sinc}^2\left(\Delta kL/2\right)$. An intensity profile of a DFG signal can be observed in Fig. 1.2.

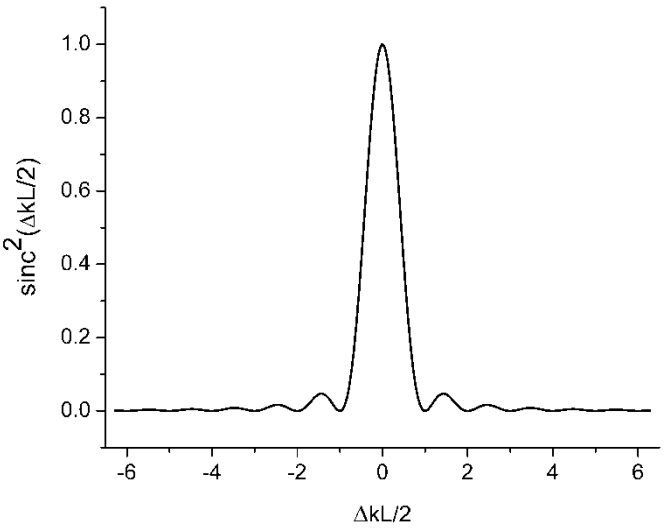

Figure 1.2. Intensity profile of DFG signal with phase mismatch. A longer sample will compress the $sinc^2$ function along the x-axis.

Single Mode Waveguide

Waveguides, or structures designed to guide electromagnetic waves, have been well studied for decades in the areas of optics and photonics. They have been important in the fabrication of fiber optic communication, light emitting diodes (LEDs), quantum cascade lasers (QCLs), and hundreds of other applications. In nonlinear DFG, the importance of a smaller cross-sectional wave comes from the property that guided waves have a much higher light intensity per area than free space traveling waves (10^5 W/mm^2 vs. 10 W/mm^2, respectively). The intensity of the generated THz wave is inversely proportional to the beam cross section, and proportional to the pump powers, as can be seen in Eq. 4.6.

A waveguide typically consists of a higher index core layer, and a lower index cladding layer. Starting with the time-harmonic Maxwell's equations

$$\Delta \times \mathbf{H} = -j\omega\varepsilon\mathbf{E} \tag{1.9}$$

$$\Delta \times \mathbf{E} = j\omega\mu\mathbf{H}\,, \tag{1.10}$$

Eq. (1.10) can be inserted into Eq. (1.9), which for a source free and lossless system will result in the wave equation:

$$\nabla^2\mathbf{E} + \omega^2\mu\varepsilon\mathbf{E} = 0 \tag{1.11}$$

where $\beta^2 = \omega^2\mu\varepsilon$. By solving the scalar Helmholtz equation perpendicular to the direction of travel, the following three solutions are obtained [8],

$$E(x) = \begin{cases} A_e \sin(hx) + A_o \cos(hx), & |x| < \frac{1}{2}d \\ Be^{-qx}, & x > \frac{1}{2}d \\ Be^{qx}, & x < -\frac{1}{2}d \end{cases} \tag{1.12a-e}$$

$$h = \sqrt{\left(\frac{n_2\omega}{c}\right)^2 - \beta_{eff}^2}$$

$$q = \sqrt{\beta_{eff}^2 - \left(\frac{n_1\omega}{c}\right)^2}$$

By solving Maxwell's equations in the three regions (low index, high index, low index), it is possible to have electromagnetic modes confined to the high index core region that satisfy Maxwell's wave equation. Each mode will have a significantly different effective index associated with it, where the effective index is an average refractive index that the mode "sees" when integrated over the high and low index material. Because the effective index of the material is important to the phase matching conditions discussed earlier, it is only possible to be phase matched to one mode. Since the fundamental mode has the highest confinement factor (thus a higher power density), the waveguide is typically designed to support only the fundamental

mode. Two main factors control the number of modes allowed to propagate; the index difference ($\Delta n = n_H - n_L$) and the thickness of the layers. Using the matrix method to calculate the effective index for the lateral and transverse directions, the dimensions were chosen such that only the fundamental IR and THz mode would propagate.

References

[1] J. F. Federici, B. Schulkin, F. Huang, D. Gary, R. Barat, F. Oliveira, and D Zimdars, "THz imaging and sensing for security applications - explosives, weapons, and drugs," *Semicond. Sci. Technol*. **20**, 266–280 (2005).

[2] S. Sattler, H. J. Hartfuss, and W7-AS Team, "Experimental evidence for electron temperature fluctuations in the core plasma of the W7-AS stellarator," *Phys. Rev. Lett.*, **72**, 653 (1994).

[3] D. Woolard, *11th Int. Space Terahertz Tech. Symp.*, Ann Arbor, MI, 22-38 (2000).

[4] F. C. de Lucia, "The submillimeter: A spectroscopist's view," *J. Mol. Spectrosc.*, **261**, 1-17 (2010).

[5] C. Staus, T. Kuech, and L. McCaughan, "Continuously phase-matched terahertz difference frequency generation in an embedded-waveguide structure supporting only fundamental modes," *Optics Express*, **16**, 13296-13303 (2008)

[6] R. W. Boyd, "Nonlinear Optics," *Academic Press*, San Diego, CA (2008).

[7] B. E. A. Saleh, and M. C. Teich, "Fundamentals of Photonics," *Wiley*, Hoboken, NJ (2007).

[8] P. Yeh, "Optical waves in layered media," *Wiley*, (2005).

Chapter 2

Advancements in $LiNbO_3$ Research

In the previous research of designing and fabricating a titanium diffused $LiNbO_3$ waveguide, it was shown that it was possible to produce phase matched, CW, and record conversion efficiency DFG Terahertz around 1.3 THz [1]. The reason for the increased power is due to tight mode confinement of the IR pumps and improved overlap between the IR and THz mode. Because the linewidth of the THz source depends only on the linewidth of the sources ($\Delta\omega_{THz} = \Delta\omega_1+\Delta\omega_2$), it is possible for the THz source to have an extremely narrow linewidth, a feature very useful in spectroscopy. To decrease the step size of the THz, increase the power, and maintain IR pump polarization, a new Erbium Doped Fiber Amplifier (EDFA) from IPG Photonics, along with other sampling equipment, was used and will be described. The following sections will describe improvements to the $LiNbO_3$ system and results produced from the advancements.

Optical System

The optical system for THz generation consisted of fiber optic cable for directional coupling of the IR pumps, and free space optics for directing/scattering and focusing of the IR pumps and THz, respectively. The purpose of the first half of the system (Fig. 2.1) was to direct the low power IR pumps (~1 - 2 mW/pump) and amplify each wavelength (~4 - 5 W/pump). In our system, we used two external cavity laser diodes (ECLDs), one polarized (variable

wavelength) and one unpolarized (fixed wavelength). Since the nonlinear coefficient depends on the polarization of the incident light and hence the THz generation, the unpolarized source was input into a polarization rotator and polarizer. The polarization rotator was used to maximize the amount of light through the polarizer. To modulate the THz source so the lock-in amplifier would detect it from the bolometer, the variable wavelength ECLD was modulated with an external sine wave (f = 10 Hz) signal from the function generator, effectively modulating both sources with opposite phase where the product of the two sources have the form

$$P_{THz} = \eta P_1(\omega_1) P_2(\omega_2) = \eta \left(\frac{P_{EDFA}}{4} \right)^2 \left[2.5 - 0.5 \cos 4\pi f_o t + 2 \cos 2\pi f_o t \right] \qquad (2.1)$$

where the lock-in amplifier can locked onto either the 1f or 2f signal. Once both sources where polarized, the signals were coupled into a 3 dB splitter, where half of the signal went into an optical spectrum analyzer for observation, and the other half went into the erbium doped

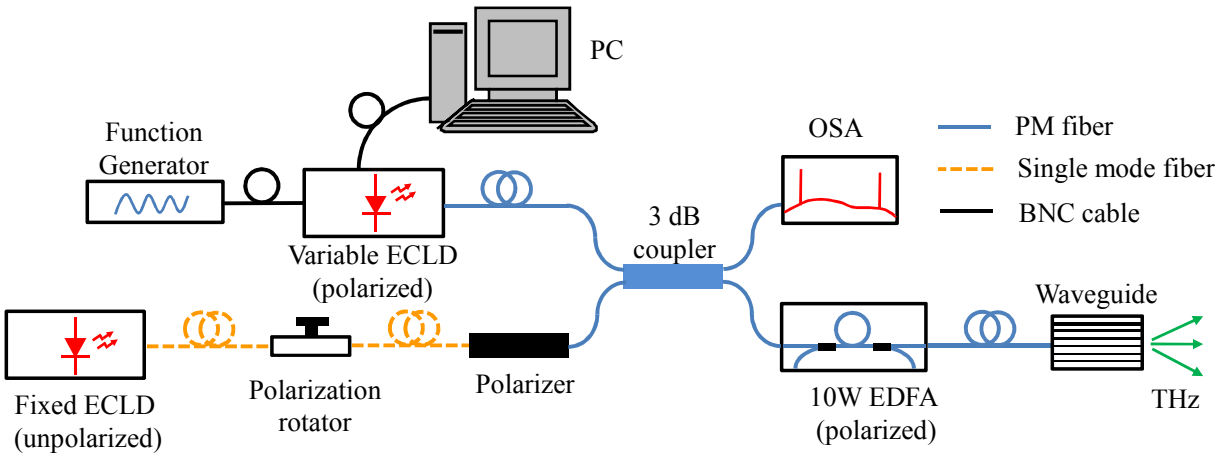

Figure 2.1. Optical circuit diagram for THz generation. ECLD (External Cavity Laser Diode), OSA (Optical Spectrum Analyzer), EDFA (Erbium Doped Fiber Amplifier), and PM (Polarization Maintaining).

amplifier (EDFA) for amplification. The output of the EDFA was a collimated, polarized beam, which was focused into a PM single mode fiber using a lens with an anti-reflecting IR coating (Thorlabs). Once coupled into the fiber, it was directed into the $LiNbO_3$ waveguide using a PM fiber.

The second half of the optical system dealt with focusing the THz beam into the liquid helium cooled bolometer and analyzing the two IR pump frequencies and equalizing the two pump powers for maximum THz generation (Fig. 2.2). If the phase matching condition is met, the output of the waveguide will consist of spatially overlapping IR and THz light. An HDPE lens was used to scatter most of the IR light and focus the THz light. Once through the 74 cm steel sample chamber, the THz and remaining IR would pass through a 5 mm HDPE plate and a 300 μm black HDPE film to block the remaining IR into the liquid helium cooled bolometer. The THz signal was detected by the lock-in amplifier and sent to the PC for data acquisition. Because the 1f signal could be four times larger than the 2f signal (2:0.5), the lock-in was set 1f. To ensure both IR pumps were set to produce the maximum THz signal, a free space optical system was designed to monitor both pump signals. A 90% transmission Pellicle beam splitter redirected part of the IR pump. Another Pellicle beam splitter redirected part of the IR light into a Spiricon CCD camera to monitor the coupling of the PM fiber into the waveguide. The rest of the IR light was sent to a diffraction grating which spatial separated the two IR wavelengths. Two 2 mm Ge photodiodes were used to detected the spatially separated IR signals. Using a 10k resistor in parallel with the photodiode, the voltage was sampled using an NI-6008 DAQ device and monitored by the PC. As the wavelength of the variable ECLD was changed, the relative powers between the two IR signals would also change, so to compensate the optical power of the fixed

ECLD was altered to equalize the two pump powers. Examples of the three possible situations for the IR pumps are displayed in Fig. 2.3.

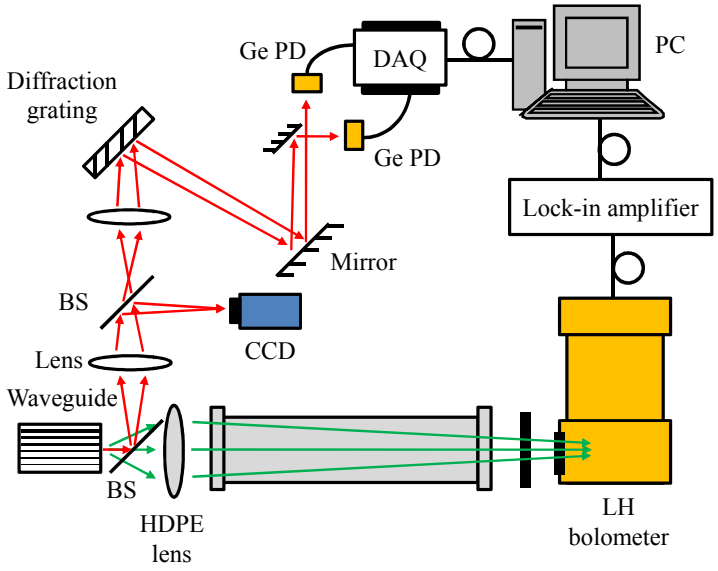

Figure 2.2. Free space optical circuit diagram for THz detection. BS (Beam Splitter), HDPE (High Density Polyethylene), LN (Liquid Nitrogen), CCD (Charge-Coupled Device for measuring IR), Ge PD (Germanium Photodiode), and DAQ (Data Acquisition device).

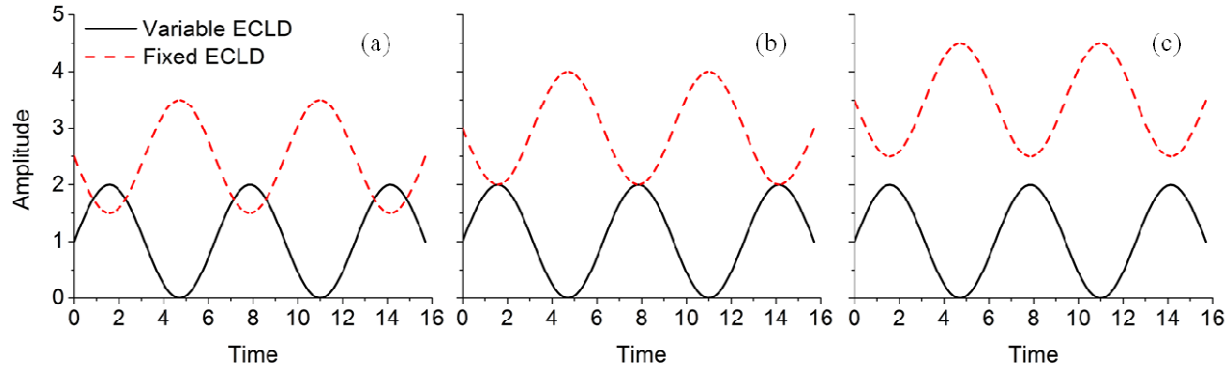

Figure 2.3. Compilation of possible relative ECLD powers at output of EDFA. (a) ECLDs overlap, decreasing 1f component and increasing 2f component. (b) ECLDs equal, 1f maximum, optimal situation. (c) ECLDs separation, decreasing 1f and decreasing 2f.

The major improvements over the previous system for THz generation are the maintaining of the IR pump polarization, increased IR power into the waveguide, two narrow linewidth IR sources, equalizing pump frequency power, and automation of scanning the IR pump wavelengths. For the DFG process, the polarization of the incident pump light is important because of the birefringence of $LiNbO_3$ and the nonlinear polarization coefficient. As a result, it is important to maintain the polarization of the light through the fiber until it is coupled into the waveguide. To accomplish this, polarization maintaining fiber (PM), PM Erbium Doped Fiber Amplifier (EDFA), and polarized sources were used. As the wavelength of the variable pump varied, the polarization change was minimal (±5º), corresponding to a difference in the nonlinear coefficient of ±0.12 pm/V. A 10W EDFA was used to increase the IR pump powers since the generated THz increased as the square of the input power [1]. Because of coupling losses and Fresnel reflections, approximately 75% of the light from the EDFA was coupled into the $LiNbO_3$ waveguide. Initially, an external cavity laser diode (ECLD) and distributed feedback laser (DFB) were used as the IR pumps, where the ECLD and DFB had a typical spectral linewidth of <1 MHz and ~10 MHz, respectively. Since the spectral width of the THz is a convolution of the two pump signals, the larger linewidth DFB was replaced with a narrow linewidth ECLD to decrease the linewidth of the THz signal. In addition to the generated THz proportional to the square of the pump powers, it is also dependant on the equalization of the pumps, where it is a max when $P_1 = P_2$ since $P_3 = \eta_p P_1 P_2$, where η_p is the overall conversion efficiency.

Spectrum of CO_2 and MeOH

Spectroscopic data in the THz regime has been of increasing interest for fingerprinting of atmospheric and extraterrestrial molecules [2,3]. As a result, it has become increasingly

important to fabricate high powered, tunable, narrow linewidth, and coherent THz sources. Currently, the only high-powered sources are broadband pulsed sources and are not ideal for spectroscopy. The DFG THz signal we can produce is limited only by the linewidth and optical power of the pump sources used to generate it. In our experiments, we have used two ECLDs with ~1 MHz linewidth and amplified to a power of 4.3 W/pump, producing about ~1.3 μW of THz. To test our source, we took a spectroscopic scan of Methanol (CH_3OH) at 610 mTorr (81 Pa). The sample chamber was first evacuated and then backfilled with MeOH in an ice bath at a temperature of -49ºC using a dry ice/cylcohexanone/ethanol mixture. Fig. 2.3 is the resulting low pressure scan. To calibrate the THz frequency axis, a low pressure scan of CO was taken and the observed absorption peak compared to the actual absorption peak (1267.014 GHz) [4], resulting in a increase in x-axis frequency of ~50 GHz. At 81 Pa and Doppler broadening of 268 kHz/Pa, the absorption broadening will be 23.3 MHz, approximately 10-times larger than the spectral width of our THz source. To decrease the Doppler broadening and increase the deep absorption lines, a longer sample chamber must be used.

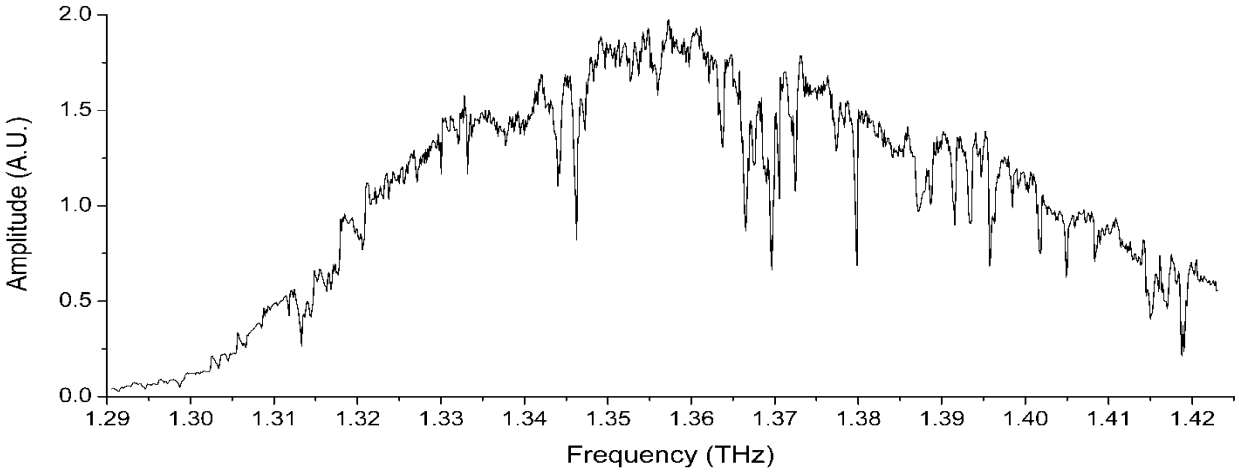

Figure 2.3.Absorption spectrum of MeOH at 680 mTorr at room temperature and 74 cm length sample chamber.

The results of our experimental absorption scan vs. other experimental data is presented in Table 2.1 [5]. Inaccuracies in the data could be a result of uncalibrated sources in the referenced work, or error in the ECLD tuning wavelength.

Ref. [5] [THz]	Fig.2.3 [THz]	Difference [MHz]
1.330284	1.330451	167
1.340244	1.340631	387
1.342884	1.343534	650
1.356852	1.357122	270
1.372998	1.3736066	609
1.388247	1.389716	1469
1.40115	1.401422	272
1.402524	1.403184	660
1.405398	1.405576	178
1.413762	1.414766	1004

Table 2.1. Compilation and comparison of experimental peaks (Fig. 2.3) and referenced data [5].

Cover Layers

To increase the tuning range of the THz source, it is possible to increase the effective index of the THz mode and the phase matching condition for the THz generation. As discussed in Chapter 1, the index of the cladding layer will impact the effective index of the mode propagating through the waveguide. As the higher index cladding layer is introduced, if we consider Eq. 1.7, as n_{THz} increases, the left hand side remains unchanged and the THz frequency (ω_{THz}) must decrease to keep both sides equal. For the cover layers, we used quartz ($n_{Qtz} = 2.11$), sapphire ($n_{sapp\_o} = 3.09$), silicon ($n_{Si} = 3.42$), and germanium ($n_{Ge} = 4.01$). The THz plot with three of the four semiconductor/crystal cover layers is plotted below. As is expected, the higher index material causes the peak THz to decrease in frequency.

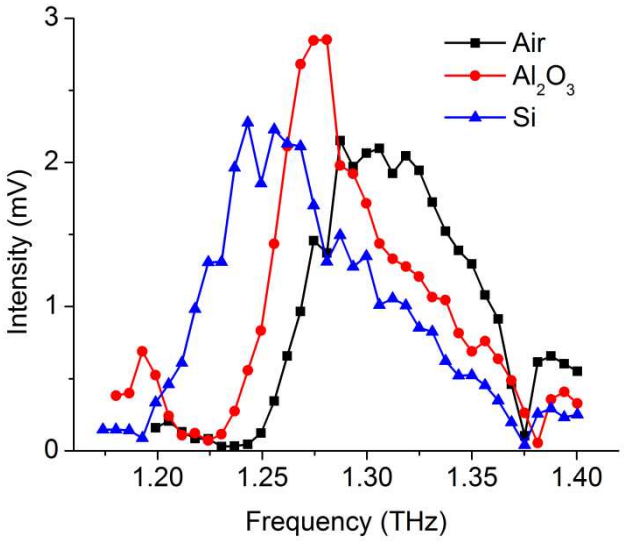

Figure 2.4. Experimental data of 6.3 GHz step scan with three different cladding layers above the $LiNbO_3$ waveguide. Air, 500 μm Al_2O_3, and 500 μm (100) Silicon.

It is also possible to increase the output power generated by the DFG process by introducing a higher index, but lower absorption cover layer. $LiNbO_3$ has a relatively high attenuation coefficient (α_{LiNbO3} = 3.02 cm^{-1}), while materials such as quartz, sapphire, silicon, and germanium have lower attenuation coefficients of α_{Qtz} = 0.5 cm^{-1}, α_{sapp} = 2.51 cm^{-1}, α_{Si} = 0.63 cm^{-1}, and α_{Ge} = 0.70 cm^{-1}, respectively. Because the THz mode is large and extends beyond the $LiNbO_3$, it is possible for the THz to act as a substrate radiation mode and leak into the higher index cover layer. An example of such mode with a 500 μm thick cover layer is shown in Fig. 2.5.

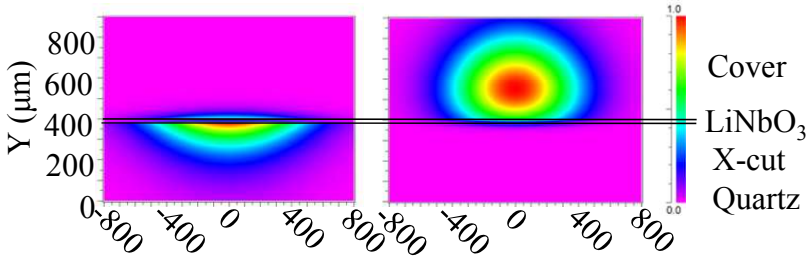

Figure 2.5. Paraxial mode propagation simulation (RSoft's BeamPROP) of the THz mode with (a) air/$LiNbO_3$/Qtz layers and (b) (100) Ge/$LiNbO_3$/Qtz layers.

References

[1] C. Staus, T, Kuech, and L. McCaughan, "Continuously phase-matched terahertz difference frequency generation in an embedded-waveguide structure supporting only fundamental modes," *Optics Express*, **16**, 13296-13303 (2008).

[2] P. H. Siegel, IEEE Trans. on Microwave Theory and Techniques, **30**, 910 (2002).

[3] C. P. Endres, , B. J. Drouin, J. C. Pearson, H. S. P. Müller, F. Lewen, S. Schlemmer, and T. F. Giesen, Astronomy & Astrophysics no. 12409, (2009).

[4] G. Winnewisser, S. P. Belov, T. Klaus, and R. Scheider, "Sub-doppler measurements on the rotational transitions of carbon monoxide," *J. Molec. Spectrosc.*, **184**, 468-472 (1997).

[5] G. Moruzzi, J. C. Silos Moraes, and F. Strumia,"Far infrared laser lines and assignments of CH3OH: a review," *International Journal of Infrared and Millimeter Waves*, **13**,1269 (1992)

Chapter 3

AlGaAs Waveguide Design

The accuracy of experimental results with the simulation of the Ti:$LiNbO_3$ waveguide for DFG Terahertz gave confidence that the current model worked well with theory. As a result, another crystalline material with nonlinear coefficient but lower absorption in the THz was chosen. Aluminum Gallium Arsenide (AlGaAs), a ternary semiconductor material was seemed ideal because there is no absorption of IR above a certain concentration of aluminum and very low absorption in the THz. Although the nonlinear coefficient of AlGaAs (d_{14} = 43 pm/V) is lower than for $LiNbO_3$ (d_{33} = 175 pm/V), the much lower absorption attributes to the higher THz power. Another reason AlGaAs was used as an alternative is the well-known processing techniques for designing ridge waveguides by decreasing the Al concentration for the core, increasing the Al concentration for the cladding, etching the ridge waveguide, and regrowth of the AlGaAs cladding layer. Also, the index of refraction for AlGaAs will phase match the IR pumps and THz around 3 THz (because of the inaccuracy of AlGaAs index of refraction in THz, the phase matching can vary between 1-5 THz, which will be examined in a subsequent section). In the following sections, the simulation, processing procedure, and testing of the AlGaAs waveguide will be analyzed. In the next chapter, the results of the experimental tests and possible reasons as to why it was not successful will be examined.

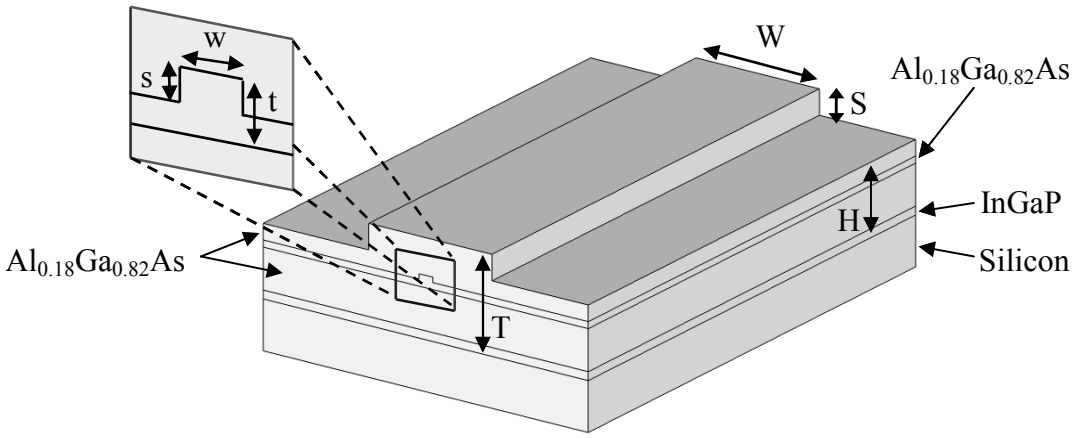

Figure 3.1. Simplified diagram of IR and THz waveguide (diagram not to scale). The small ridge waveguide is designed to confine the IR pump modes and the large ridge to confine the THz mode. The default values for s, t, and w are 1 μm, 2.5 μm, and 5 μm, respectively. The default values for S, T, and W are 15 μm, 30 μm, and 50 μm, respectively.

Configuration of AlGaAs Waveguide

Figure 3.1 shows the basic design of the nested rib waveguide in AlGaAs. The core layer was chosen to be $Al_{0.16}Ga_{0.82}As$ so it would have a higher index than the cladding layers and also have a bandgap higher than the IR pump photons to prevent against two photon absorption ($E_p = 2\hbar\omega = 1.616\,\text{eV}$ and $E_g = E_{GaAs} + E_x = 1.424 + 1.24x = 1.622\,\text{eV}$ for x=0.16) [1]. Since the bandgap of $Al_{0.18}Ga_{0.82}As$ is very close to the energy of the IR photons, it is possible for some of the photons to be absorbed into the conduction band. The dimensions were chosen such that the IR and THz modes would both be single mode. This was determined by using the effective index calculation method for rib waveguides, as briefly discussed in the first chapter.

To test that the AlGaAs waveguide was indeed single mode as the calculations and modeling predicted, IR light was coupling into the AlGaAs pump waveguide. The results of the coupling are displayed in Fig. 3.2. Both images show good single mode output from the

waveguide, but the right image shows IR light coupling into nearby waveguides, indicating the fiber/waveguide gap is large.

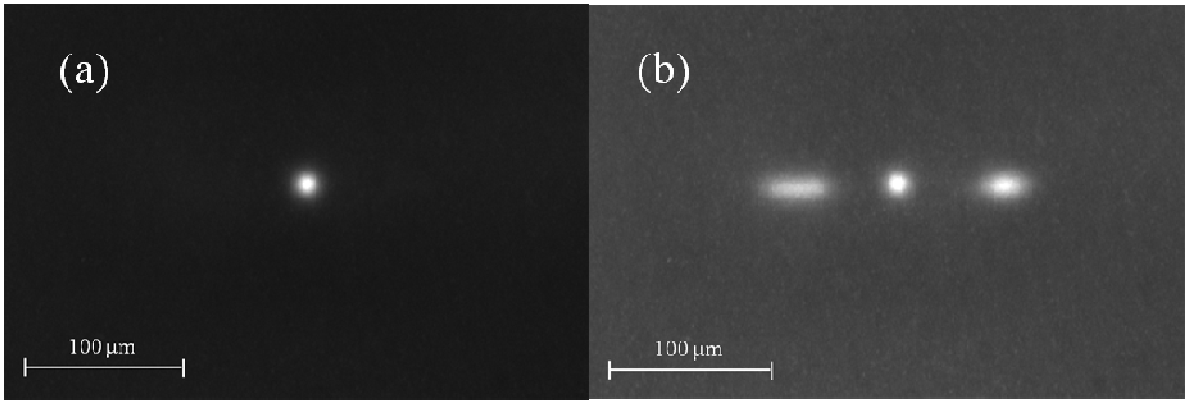

Figure 3.2. Image captured from Spiricon CCD IR camera. (a) Good coupling and single mode from AlGaAs waveguide. (b) Poor coupling between fiber and AlGaAs waveguide (~20 μm spacing). Some light scattered into adjacent waveguides.

Facet Damage

Once the IR pump light was coupled into an AlGaAs waveguide, the input power was steadily increased by 0.2 W increments. Catastrophic failure occurred at 3 W and 6.4 W, corresponding to power densities of 6.2 W/cm^2 and 13.2 W/cm^2, respectively. It has been reported that damage thresholds of 6-13 W/cm^2 have been observed in AlGaAs waveguides [1]. By applying a λ/4 coating at 1.55 μm wavelength, it is possible to increase the damage threshold above 10 W (20.6 W/cm^2). The reason for the increase of the damage threshold by applying the AR coating could be the smoothing of striations or defects present at the facets. If the facets are not perfectly cleaved, striations can be present over the waveguide and can be sources of localized heating. At these power densities (~ 20 W/cm^2), thermal expansion could cause the defects to expand and eventually cause the damage in Fig. 3.3.

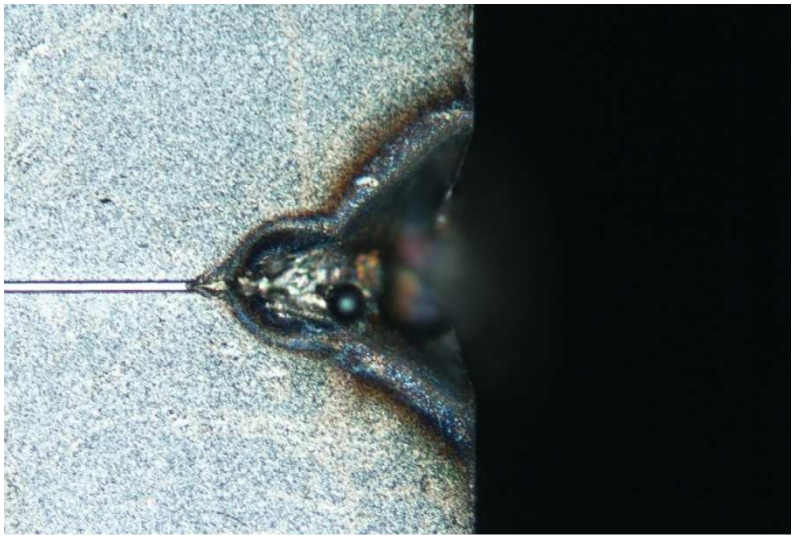

Figure 3.3. Catastrophic damage of the AlGaAs waveguide. The damage was localized to the front facet and did not affect neighboring waveguides.

IR AR coating

As will be discussed in a subsequent section, dielectric boundaries where the refractive index are different causes a partial reflection and transmission. The degree of reflection is proportional to the index difference between the material. At normal incidence, the amplitude of the reflected light can be calculated by

$$R_{IR} = \left(\frac{n_{AlGaAs} - n_{air}}{n_{AlGaAs} + n_{air}}\right) \tag{3.1}$$

where the refractive index of AlGaAs in the IR is $n_{AlGaAs} = 3.334$, causing a reflection of 30% at one interface, and a total reflection of 50% from both surfaces. A reduction of 1/2 the IR power means a reduction of 1/4 the generated THz. A common solution to decreasing the amount of reflected light is to use a antireflection coating (AR) where the index of the AR coating is λ/4 wavelength and the geometric mean of the two materials ($n_{AR} = \sqrt{n_1 n_2} = 1.826$). Three possible thin film coatings that have refractive index values close to the theoretical value and can be

applied through an evaporative deposition process are Si_3N_4, ZnO, and SiO. The thin film material we will be using is SiO because it has the lowest reflection (< 0.2%) at the desired wavelength range. An issue with using SiO is oxidation, which could increase the refractive index and increase the amount of reflected light.

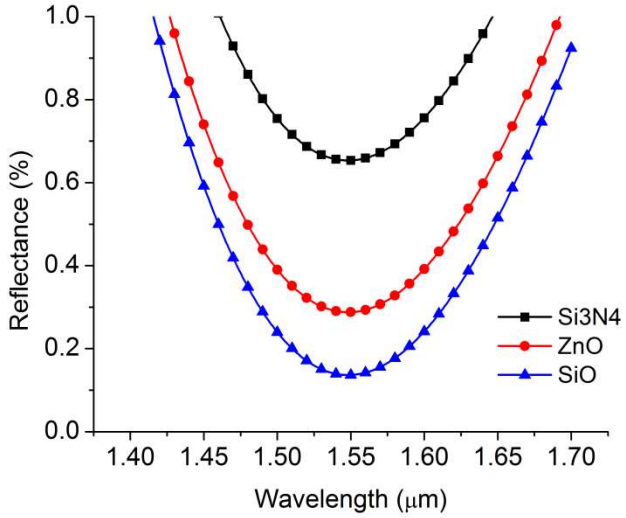

Figure 3.4. Percent reflection of incident beam with quarter wavelength film (d ≈ 200 μm) centered at λ = 1.548 μm. The wavelengths we will be using are 1.535 μm to 1.565 μm.

THz AR coating

To decrease the reflected THz light at the distal end of the waveguide, an AR can also be applied for the THz generated light. Designing and fabricating an AR coating in the THz frequency region is more difficult than for the IR because of the lack of low absorption materials, lack of knowledge of the refractive index, and large thicknesses required for λ/4 wavelength layers (10 - 100 μm). Polymers, such as HDPE (C_2H_4), could be used because of the relatively low absorption (~ 1 cm^{-1}), but the intense IR beams could damage the polymer. Crystal materials such as sapphire and quartz would be more likely candidates [2]. One method that has been used

to create thin films for THz AR coatings is mechanical lapping [3]. Quartz has a refractive index similar to the geometric mean between air/AlGaAs ($n_{AR} = \sqrt{(1)(3.6)} = 1.9 \approx$ 2.136) and low absorption (α_{Qtz} = 1.3 cm^{-1}). At a quarter wavelength thickness (10.6 μm), the calculated reflectance would be 1.2% with an absorption loss of 0.1%.

References

[1] M. Ettenberg, H. S. Sommers, Jr., H. Kressel and H. F. Lockwood, "Control of facet damage in GaAs laser diodes," *Appl. Phys. Lett*. **18**, 571 (1971).

[2] K. Kawase and N. Hiromoto, "Terahertz-wave antireflection coating on Ge and GaAs with fused quartz," *Applied Optics*, **37**, 10,1862-1866 (1998).

[3] K. Kawase, N. Hiromoto, and M. Fujiwara, "Terahertz-wave antireflection coating on Ge wafer using optical lapping method," *Electronic and Communications in Japan*, **83**, 260-264 (2000).

Chapter 4

AlGaAs Results

Although current experiments did not yield experimental results of THz from the AlGaAs waveguide, the following section will discuss possible means of frequency tuning by adjusting the waveguide dimensions and altering external structures. The first method to alter the THz peak frequency is to redesign the IR pump and THz waveguides. Although easy to do in simulation, it would be much more time-consuming and difficult in fabrication. Instead, it would be much easier to use an original design and alter the exterior structure (i.e. higher index cover layer, angle tuning, etc.). The following section will discuss possible methods of tuning by changing the thickness of the silicon substrate layer and the addition of high index cover layers. Lastly, the possible reasons as to why no experimental measurements of a THz DFG signal was detected will be discussed.

Losses in IR and THz

In semiconductor waveguide design, there are multiple factors for losses and absorption. In the AlGaAs waveguide we discuss in this paper, we report the theoretical losses associated with mode mismatch and misalignment, free carrier concentration, Fresnel reflection, and scattering/absorption.

Early methods for introducing high powered lasers into a crystalline material to produce nonlinear effects involved focusing a high powered light source into bulk material. The problem

is focusing the beam into a small cross-section which has a limit to the waist size and the beam is focused over a limited distance. To maintain a high power density over a long distance (~1 cm), it is necessary to couple the pump light into a waveguide. In this case, we will be analyzing the losses associated with the coupling of a polarization maintaining single mode fiber to a nested rib waveguide. The cause for losses in the IR pump waveguide will be longitudinal separation between the fiber and waveguide, mode mismatch, and Fresnel reflection. Table 4.1 reports the measured output from the IR pump AlGaAs waveguide.

Input power	0.5 W	1 W	1.5 W
Output power	~ 40 mW	~ 80 mW	~ 120 mW
Loss (dB)	~ -11 dB	~ -11 dB	~ -11 dB

Table 4.1. Measured output power from AlGaAs waveguide with respect to input power (input power is total of both pumps).

To prevent the AlGaAs waveguide from coming in contact by thermal expansion with the PM fiber and causing catastrophic damage, a small separation (~10 μm) is placed between the fiber and waveguide. This small distance can cause a longitudinal misalignment and can be calculated by

$$\alpha(dB)_{long} = -10\log\left(\frac{1}{\tilde{Z}^2+1}\right) \tag{4.1}$$

where

$$\tilde{Z} = \frac{Z\lambda}{2\pi n_1 w^2} \tag{4.2}$$

where Z is the length of the separation in air ($Z \approx 10$ μm), λ is the free space wavelength of the IR pumps ($\lambda \approx 1.55$ μm), n_1 is the refractive index of the fiber at λ ($n_1 = 1.45$), and w is the radius

of the single mode fiber (w ≈ 5 μm). At this distance, the calculated loss from longitudinal misalignment is $\alpha(dB)_{long}$ = -0.02 dB, accounting for a very small loss.

Another source for loss is mode mismatch. Inherently, the IR mode in a single mode fiber and nested rib waveguide do not match perfectly, causing a small amount of scattering. Using RSoft's BeamPROP simulation software, we were able to estimate the mode field diameter (MFD) of the single mode fiber and nested rib waveguide. We can then use the equation below to calculate the loss

$$\alpha(dB)_{mode} = -10\log\left(\frac{4}{\frac{w_1}{w_2}+\frac{w_2}{w_1}}\right) \tag{4.3}$$

where w_1 = 10.5 μm and w_2 = 9.7 μm. The loss from mode mismatch is $\alpha(dB)_{mode}$ = -0.03 dB, also a very small loss.

At dielectric boundaries, a fraction of light is reflected and transmitted that depends on the index difference between the two interfaces. At normal incidence, the amplitude of the reflected wave is

$$R_{IR} = \left(\frac{n_{AlGaAs}-n_{air}}{n_{AlGaAs}+n_{air}}\right). \tag{4.4}$$

Because the index difference between air and AlGaAs is relatively large, Fresnel reflection will reflect a large portion of the incident light. At λ = 1.55 μm, n_{AlGaAs} = 3.334 and n_{air} = 1. For one surface, the reflected light is R_{IR} = 0.29. The total loss for both surfaces is: $1-T^2 = 1(1-R^2) \approx 0.5$ or $\alpha(dB)_{Fresnel}$ = -3 dB.

A source of loss in the IR pump wavelengths is absorption by free carriers. Free carrier absorption (FCA) arises from unintentional doping of the semiconductor material. The absorption coefficient from FCA is given by [1]

$$\alpha_{FCA} = \frac{Nq^2\lambda^2}{\varepsilon_o m_{eff} 4\pi^2 nc^3 \tau} \quad (4.5)$$

where N is the free carrier concentration (< 10^{-16} for our current prototypes), n is the refractive index (~ 3.3 in the IR frequency), τ is the relaxation time constant (~ 0.6 ps in $Al_{0.18}Ga_{0.82}As$), and m_{eff} is the carrier effective mass (~ 0.08*$m_{electron}$) [2]. The results of the FCA are tabulated in Table 4.2.

Free carrier concentration (cm^{-3})	10^{15}	10^{16}	10^{17}	10^{18}	10^{19}
Attenuation (cm^{-1})	7.04×10^{-5}	7.04×10^{-4}	7.04×10^{-3}	0.0704	0.704

Table 4.2. Attenuation of THz guided mode with respect to free carrier concentration.

Lastly, another source for IR loss is scattering/absorption internal to the nested rib waveguide. Although directly difficult to experimentally measure, if the previously discussed sources of loss are taken into account, the remaining loss must be attributed to loss or absorption. Since the total loss is ~ -11 dB, and the majority of the calculated loss is due to Fresnel reflection (-3 dB), the remaining loss due to scattering/absorption is ~ -8 dB.

To determine the optimal length and effect of the free carrier absorption on the generated THz, the closed form expression by Aggarwal and Lax was used (Eq. 4.6) [3].

$$P_{THz} = \frac{1}{2}\sqrt{\frac{\mu_o}{\epsilon_o}}\left(\frac{4\omega_{THz}{}^2 d_{14}^2 L^2}{n_1 n_2 n_{THz}}\right)\left(\frac{1}{c^2}\right)\left(\frac{P_{\omega_1}P_{\omega_2}}{A}\right)\left(e^{-\alpha_{THz}L}\right)\left(\frac{1+e^{-\Delta\alpha L}-2e^{-\frac{1}{2}\Delta\alpha L}}{\left(\frac{1}{2}\Delta\alpha L\right)^2}\right) \quad (4.6)$$

In this equation, $n_{1,2,THz}$ are the effective indices of the structure at the two pump frequencies $f_{1,2,THz}$. The second order nonlinear coefficient is d_{14} = 43 pm/V. The losses in the IR and THz are represented by $\alpha_{1,2,THz}$ ($\Delta\alpha = \alpha_1 + \alpha_2 - \alpha_{THz}$). The device length is defined by L and the pump

wavelengths are nominally 1.55 μm. Fig. 4.1 shows the effects of the FCA on the generated THz as a function of length. Based on the reported free carrier concentration of the AlGaAs samples by Sumika, a sample with a length of ~7.2 cm will produce a maximum of coherent, tunable THz light.

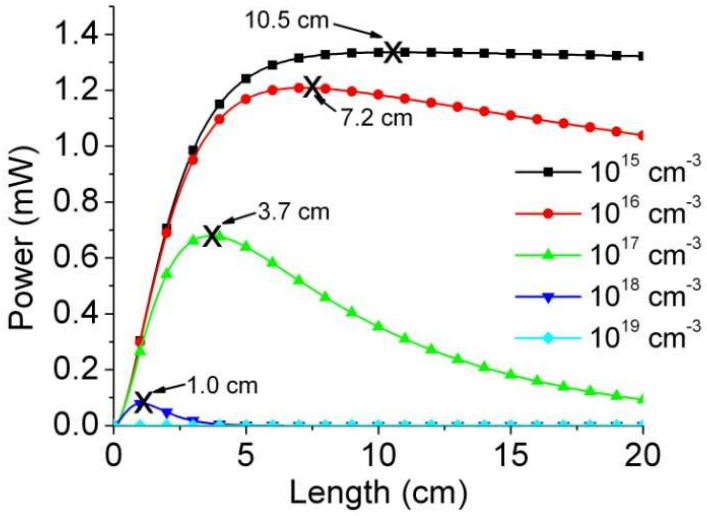

Figure 4.1. Maximum generated THz as a function of free carrier concentration and length. The calculation is based on pump powers of 4 W each. The maximum interaction length is indicated on the graph.

The total THz peak power will be decreased as a direct result of the losses in the IR pump powers. If we use the minimum measured pump light in the waveguide ($P_1 = P_2 = 80$ mW), we expect to measure a signal of $P_{THz} = \eta P_1 P_2 = 83$ nW ($\eta = 1.3 \times 10^{-5}$). Subtracting the losses from the THz imaging system and bolometer filters, we would expect to measure a signal of 18 mW, where the noise floor is approximately 1.5 mW.

Alteration of AlGaAs Waveguide

By altering the thickness of the IR and THz waveguides, the mode profile and the effective index of the mode will be altered, changing the location of the peak THz power. The first parameters we will consider will be the s, t, and w values for the IR waveguide. The results of altering the thicknesses are plotted below (Fig. 4.2-4.4).

As we can see, increasing any of the s, t, or w parameters has a tendency to increase the THz peak frequency by several 10s of GHz. If we consider the phase matching requirement ($n_1\omega_1 - n_2\omega_2 = n_T\omega_T$), increasing the IR pump waveguide cross-section will increase the effective index of the pump mode. According to the previous equation, if n_1 and n_2 increase and n_T remains fixed, then ω_T will increase to keep both sides of the equation equal. The limits to such changes are defined by introducing higher modes to the waveguide or mode mismatch between the fiber coupled to the waveguide. Mode mismatch was discussed in a previous section.

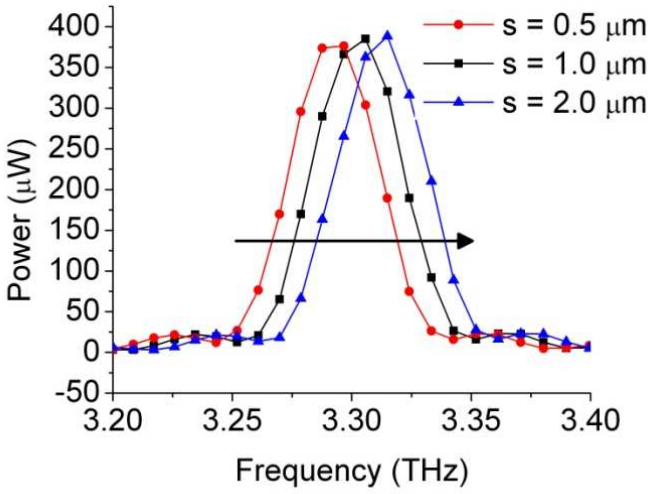

Figure 4.2. Effect of changing the rib height of the IR pump waveguide. The peak power remains constant but the peak THz frequency increases as the height increases.

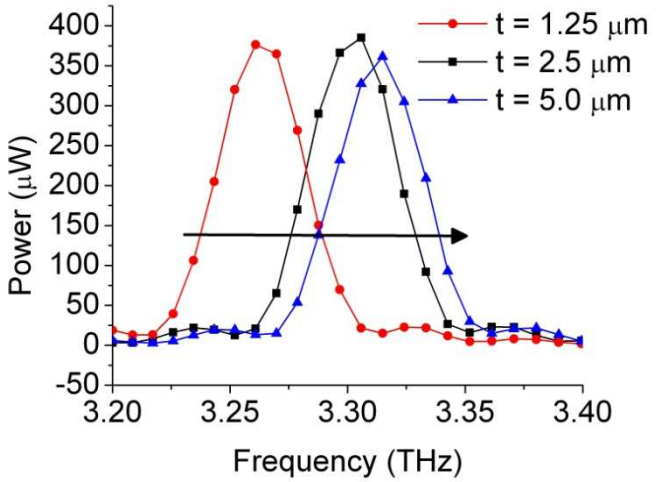

Figure 4.3. Effect of changing the rib and slab height of the IR pump waveguide. The peak power remains constant but the THz frequency increases as the height increases.

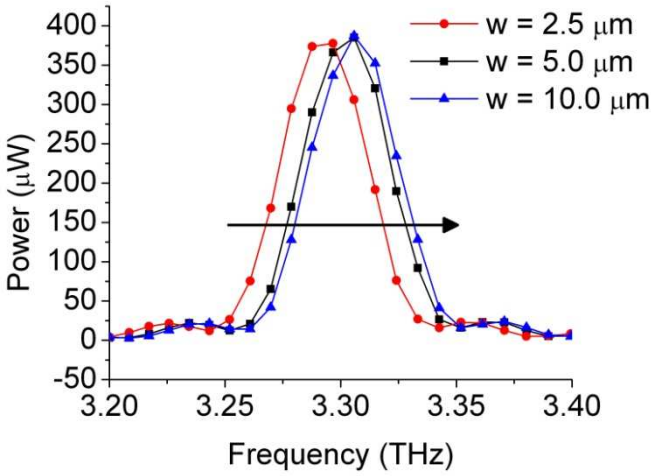

Figure 4.4. Effect of changing the rib width of the IR pump waveguide. The peak power remains constant but the peak THz frequency increases as the width increases.

As was just discussed, altering the IR pump waveguide dimensions shifted the THz peak in frequency. If we apply the same principle to the THz waveguide, a frequency shift should also

be observed. In the following three plots, the physical dimensions S, H, and W are altered and the effects plotted in Fig. 4.5-4.7.

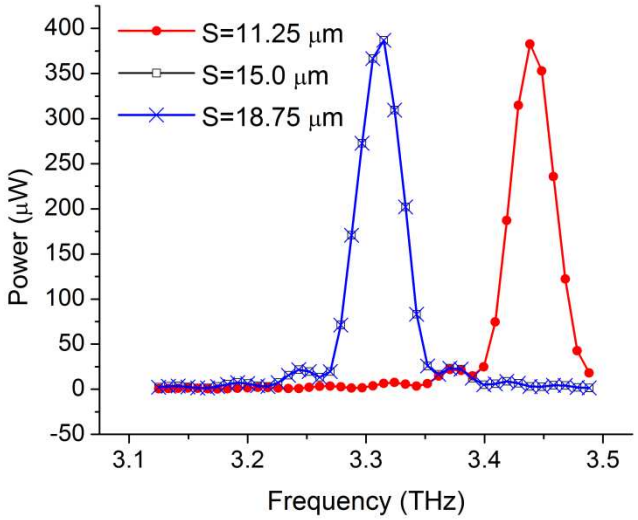

Figure 4.5. Effect of changing the ridge height of the THz waveguide. Decreasing the height below 15.0 μm had no effect but increasing it above 15.0 μm increased the THz frequency.

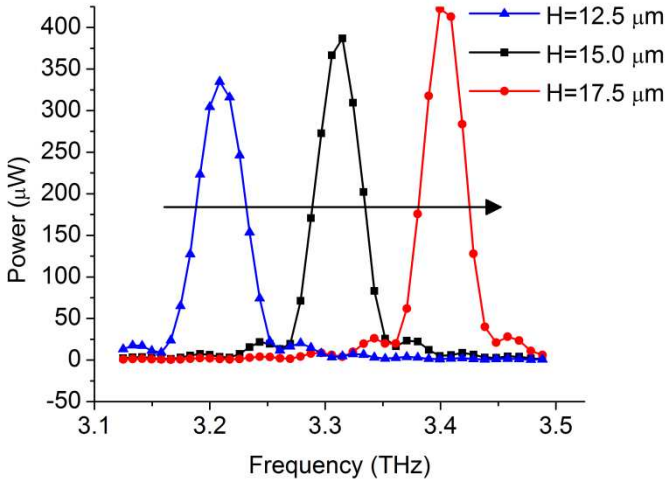

Figure 4.6. Effect of changing the slab height of the THz waveguide. Increasing the slab thickness increased the peak THz frequency and also the peak power.

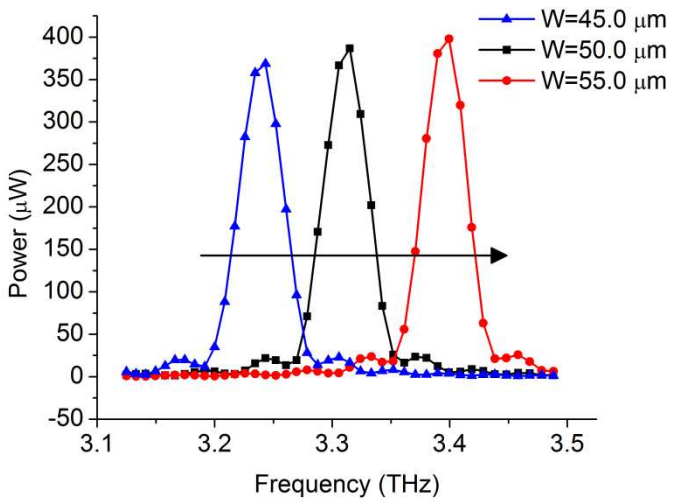

Figure. 4.7. Effect of changing the slab width of the THz waveguide. Increasing the slab width increased the peak THz frequency while the peak power remained constant.

By adjusting the IR pump and THz waveguide dimensions, it is possible to create a widely tunable THz source over 100s of GHz. This flexibility in tuning would have a major impact on molecular and astronomical spectroscopy for fingerprinting molecules. More methods for increasing the tuning range without directly altering the physical parameters are presented in the next section.

Advanced AlGaAs Structures

Because it may be unreasonable to design and build a new structure each time a different wavelength is required, it would be advantageous to alter external parameters for tuning the THz frequency. A couple methods to accomplish this would be to thin the Silicon substrate layer or apply a higher index cover to the waveguide. Examples of this method are displayed in Fig. 3.9.

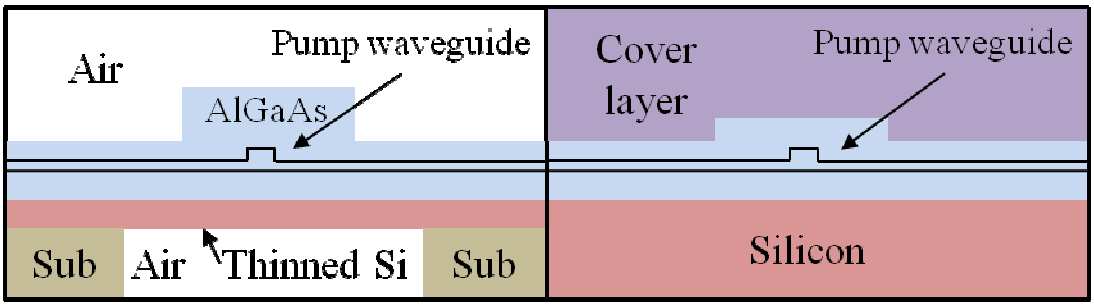

Figure 4.8. Diagram of AlGaAs waveguide placed on thinned Silicon substrate (left) and replacing air cover layer with higher index material (right).

In the left hand side of Fig. 4.8, the THz mode becomes more confined to the Si and AlGaAs waveguide. By adjusting the thickness of the Silicon substrate, the effective index of the THz mode can be changed. As the Silicon layer is thinned, the peak THz frequency increases (Fig. 4.9). Therefore, the original structure can remain unchanged while the substrate on which it lays can be changed. In the right hand side of Fig. 4.8, a material with an index > 1 is placed over the AlGaAs waveguide. As was observed in the $LiNbO_3$ experiment work, this effectively lowers the peak THz frequency (Fig. 4.9).

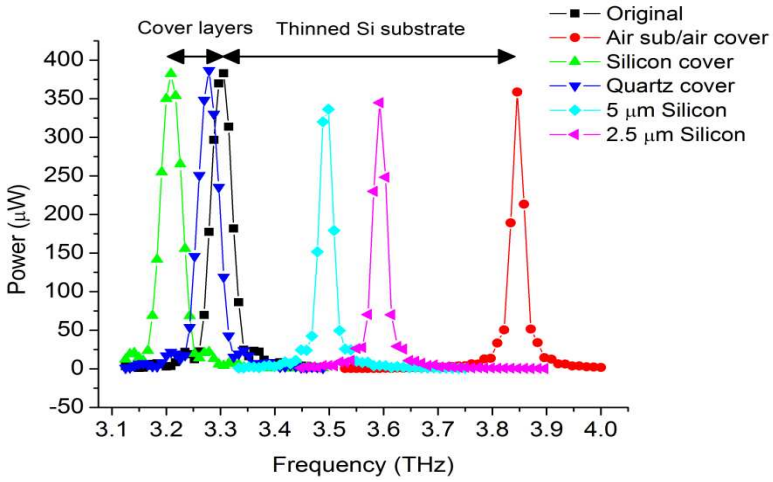

Figure 4.9. Composite of methods for shifting the peak THz frequency to higher or lower frequencies by thinning the Silicon layer or adding a higher index material, respectively.

Possible materials to use as cover layers are silicon, quartz, sapphire, and germanium. By adding the cover layer, more of the THz mode "sees" the material and propagates partially inside the AlGaAs guide and cover material. If the cover layer has a higher index than the AlGaAs waveguide in the THz frequency, such as germanium, the THz mode will "leak" into the higher index material as a substrate radiation mode. Since the absorption coefficient of germanium [4] is lower than AlGaAs [5] at 100 μm, not only would the peak THz be at a lower frequency but also higher power.

References

[1] S. Adachi, "GaAs, AlAs, and $Al_xGa_{1-x}As$ material parameters for use in research and device applications," *J. Appl. Phys.*, **58**, R1-R29 (1985).

[2] C. M. Wolfe, N. Holonyak Jr., G. E. Stillman, "Physical Properties of Semiconductors," 226 (1989).

[3] R. L. Aggarwal and B. Lax, "Optical mixing of CO_2 lasers in the far-infrared," *Applied Physics*, **16**, 19-80 (1977).

[4] R. F. Potter, "Germanium," *Elsevier*, 478 (1998).

[5] S. Adachi, "Properties of Aluminum Gallium Arsenide", 198 (1993).

Chapter 5

Conclusion

Designing and fabricating a THz source by difference frequency generation is difficult because of the spatial overlapping of the pump sources and generated THz field, low conversion efficiency as defined by the Manly-Rowe limit ($\omega_3/\omega_1 \approx 10^{-2}$ for THz DFG from IR pumps), poor overlap between the fields, high absorption in materials, and lack of accurate refractive index knowledge in the THz regime. Because of the low THz power generated, the only good detectors are liquid-helium cooled bolometers, which can be difficult to use and are unreasonable for practical applications. As a result, there is a major push for designing and fabricating higher powered THz sources or more practical THz detectors. The goal of this research project was to increase the conversion efficiency of the THz source and increase the THz power some 80 times more than the previously developed sources. Unfortunately, we were unable to successfully detect a THz signal. There are multiple possibilities for this which will be discussed in the next section.

Uncertainties and Error

Because the photon energy in the THz regime is so small (0.0012 eV - 0.012eV), it is difficult to create sources that will generate that low of energy photon. A well known process to produce THz and other far-IR sources is using nonlinear material where the polarization depends nonlinearly on the incident electric field. Sources are typically required need to have intensities of 10^8 V/m. The nonlinear process used to generated a THz frequency source is the frequency

mixing process of difference frequency generation (DFG), where the phase matching condition is defined by the following equation

$$n_1\omega_1 - n_2\omega_2 = n_T\omega_T \tag{5.1}$$

where $n_{1,2}$, $\omega_{1,2}$ are the refractive index and frequency of the IR pumps sources, and n_T, ω_T are the refractive index and frequency of the THz. At these frequencies, the refractive index is typically calculated by using the Kramers-Kronig relation using the absorption data to calculate the refractive index. A small error in the actual refractive index can have a large impact on the phase matching of the DFG process. If we consider an error in the refractive index, Δn_T, we can modify Eq. 5.1 to account for the error.

$$n_1\omega_1 - n_2\omega_2 = (n_T \pm \Delta n_T)\omega_T \tag{5.2}$$

If we take $\Delta n_T = 0.1$, the error in the refractive index can change the peak THz by ±300 GHz. Because of the limitations of our EDFA, it could easily push the THz to a frequency unattainable by our current equipment.

Another reason the THz signal was not detected could be from the high absorption in atmosphere. At a distance of 1 meter from source to bolometer, approximately the distance the $LiNbO_3$ scan was measured, there are several strong absorption lines in the frequency of interest (Fig. 5.1). If the THz signal was generated in any one of these absorption lines, it would not be detected.

Finally, it is possible that the nonlinear coefficient used for GaAs (43 pm/V) cannot be assumed for $Al_{0.18}Ga_{0.82}As$, resulting in a much smaller 2nd order nonlinear process.

Although the AlGaAs waveguide did not produce a detectable THz signal, we are still in the process of determining the cause and theorizing possible solutions.

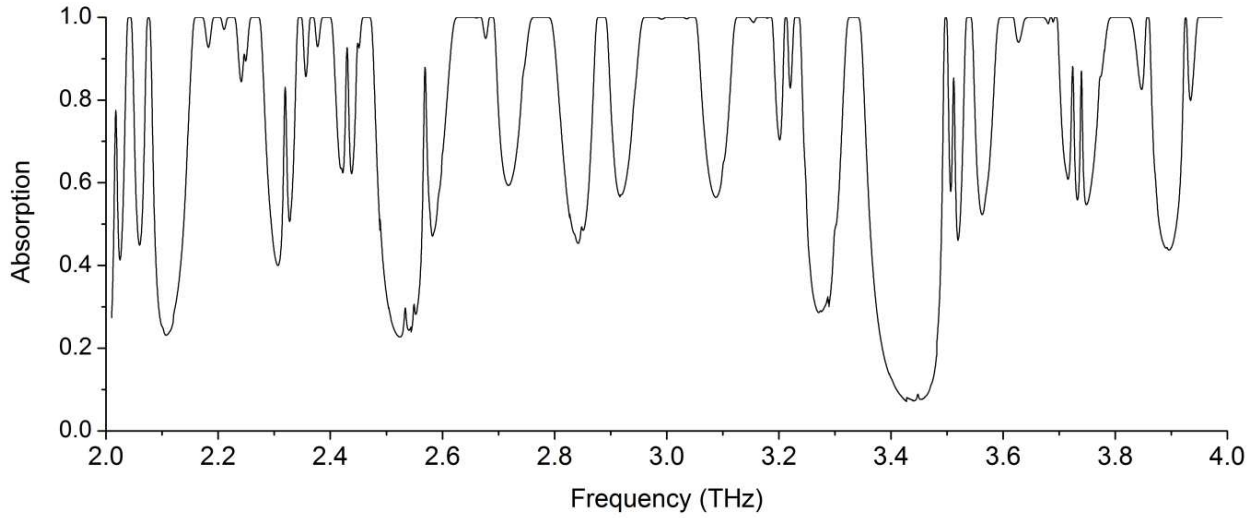

Figure 5.1. Calculated absorption scan of atmosphere at 1 meter. Notice there are only a few narrow windows where the THz would not be completely absorbed [1].

References

[1] HITRAN/GEISA, "Spectroscopy of atmospheric gases," (2011).